Physical and Mechanical Degradation Behaviour of Semi-Crystalline PLLA for Bioresorbable Stent Applications

Katarzyna Polak-Kraśna[a*], Ali Reza Abaei[a], Reyhaneh Neghabat Shirazi[a], Eoin Parle[a1], Oliver Carroll[b], William Ronan[a], Ted J. Vaughan[a*]

[a] Biomechanics Research Centre (BioMEC), Biomedical Engineering, School of Engineering, College of Science and Engineering, National University of Ireland Galway, Galway, Ireland

[b] CÚRAM, Centre for Research in Medical Devices, Biomedical Sciences, National University of Ireland Galway, Galway, Ireland

*corresponding authors:

Dr. Katarzyna Polak-Kraśna
Lecturer in Biomedical Engineering,
Biomechanics Research Centre (BioMEC),
Biomedical Engineering,
National University of Ireland Galway,
Galway,
Ireland
Phone: (353) 91-492538
Email: k.polak-krasna@nuigalway.ie, polak.krasna@gmail.com

Dr. Ted J. Vaughan
Senior Lecturer in Biomedical Engineering,
Biomechanics Research Centre (BioMEC),
Biomedical Engineering,
National University of Ireland Galway,
Galway,
Ireland
Phone: (353) 91-493084
Email: ted.vaughan@nuigalway.ie

---

[1] Present address: Galway-Mayo Institute of Technology, Old Dublin Rd, Galway

Abstract

This study presents a systematic evaluation of the physical, thermal and mechanical performance of medical-grade semi-crystalline PLLA undergoing thermally-accelerated degradation. Samples were immersed in phosphate-buffered saline solution at 50°C for 112 days and mass loss, molecular weight, thermal properties, degree of crystallinity, FTIR and Raman spectra, tensile elastic modulus, yield stress and failure stress/strain were evaluated at consecutive time points. Samples showed a consistent reduction in molecular weight and melting temperature, a consistent increase in percent crystallinity and limited changes in glass transition temperature and mass loss. At day 49, a drastic reduction in tensile failure strain was observed, despite the fact that elastic modulus, yield and tensile strength of samples were maintained. Brittleness increase was followed by rapid increase in degradation rate. Beyond day 70, samples became too brittle to test indicating substantial deterioration of their load-bearing capacity. This study also presents a computational micromechanics framework that demonstrates that the elastic modulus of a semi-crystalline polymer undergoing degradation can be maintained, despite a reducing molecular weight through compensatory increases in percent crystallinity. This study presents novel insight into the relationship between physical properties and mechanical performance of medical-grade PLLA during degradation and could have important implications for design and development of bioresorbable stents for vascular applications.

Keywords:

1. Introduction

Bioresorbable stents (BRS) provide temporary mechanical scaffolding to an artery following implantation and are subsequently removed from the body through bioresorption. Despite early clinical data demonstrating safety and efficacy of BRS devices (Gonzalo et al., 2012; Kraak et al., 2015), two-year follow up data has shown increased risk of myocardial infarction and higher incidence of late-stage complications such as thrombosis when compared with permanent drug-eluting stent (DES) (Cassese et al., 2016; Lipinski et al., 2016; Serruys et al., 2016). There is evidence that late scaffold fracture or discontinuity could lead to late stage thrombosis (Patel et al., 2017; Sorrentino et al., 2017; Stone and Granada, 2015). This has highlighted the need for better understanding of long-term degradation behaviour and related evolution of mechanical properties of BRS materials. Poly (L-lactide) (PLLA) is by far the most commonly used bioresorbable material for BRS devices, with Absorb (Abbott Vascular, Santa Clara, CA, USA), DeSolve (Elixir Medical, Sunnyvale, CA, USA), Amaranth (Amaranth Medical Inc., CA, USA), Acute BRS (Orbus Neich, Fort Lauderdale, FL, USA) and the Igaki-Tamai stent (Kyoto Medical Planning Co, Ltd, Kyoto, Japan) all made from this polylactide-based polymer. Although there is limited experimental data on medical-grade PLLA in the public domain, studies have reported a wide variation in mechanical performance across PLLA-based materials (Bartkowiak-Jowsa et al., 2013; Dreher et al., 2016; Hayman et al., 2014; Kimble and Bhattacharyya, 2015; Nuutinen et al., 2003; Soares et al., 2008; Tsuji, 1995; Tsuji and Ikada, 2000; Venkatraman et al., 2003; N. . Weir et al., 2004; N. A. Weir et al., 2004a, 2004b; Zilberman et al., 2005) and devices (Grabow et al., 2007; Luo et al., 2014; Nuutinen et al., 2003; Qiu et al., 2018; Venkatraman et al., 2003; Zilberman et al., 2005) undergoing degradation. These differences are driven by variations in either the polymer composition or processing parameters used during manufacturing (Grabow et al., 2005). Together, these are responsible for the polymer's bulk microstructural properties (e.g. molecular weight, degree of crystallinity, crystal morphology), which in-turn dictate mechanical properties (e.g. stiffness, strength, ductility) and overall degradation kinetics such as degradation rates at different stages of the process. A major challenge to improving long-term properties of bioresorbable devices is understanding how temporal changes to the polymer's bulk microstructure governed by degradation kinetics precisely influence overall mechanical performance during degradation.

PLLA is a semi-crystalline material that degrades *in vivo* through bulk degradation (Antheunis et al., 2009). This initiates in the amorphous regions of the polymer microstructure, whereby hydrolysis of ester bonds in the polymer chains takes place, with the resulting degradation products metabolised by the body. Polymer chain scission sees the molecular weight of the polymer decrease, with either number average (M_n) or weight average (M_w) measures of this parameter widely used as a key indicators of degradation behaviour. In many cases, a direct relationship between molecular weight and mechanical properties of degrading amorphous polymers has been observed (Farrar and Gillson, 2002; Gleadall, 2015) and theoretical models have been proposed to provide predictions of physical and mechanical behaviour (Shirazi et al., 2016; Wang et al., 2010). However, this relationship does not translate to semi-crystalline materials. Crystalline phases are characterised by highly-ordered compact structures of polymer chains that heavily influence the mechanical response, in particular contributing to stiffness and strength of the polymer. Importantly, during the hydrolytic degradation process, the amorphous phase is penetrated by water molecules causing chain-scission, which provides shorter polymer chains with extra mobility that faciliatates new crystallite regions to form (Wang et al., 2008a). This means that the effective degree of crystallinity during degradation of PLLA will actually increase (Dreher et al., 2016; N. A. Weir et al., 2004a). This presents a complex evolving relationship between molecular weight, degree of crystallinity and mechanical performance of the polymer throughout the degradation process. Several authors have proposed useful physio-chemical models that use a reaction-diffusion frameworks to investigate the effect of crystallinity on degradation kinetics and the evolution of the molecular weight (S. P. Lyu et al., 2007; Wang et al., 2008b). However, very few physical models have been linked to mechanical performance and, to date, mechanical-based degradation modelling of semi-crystalline polymers has been largely phenomenological (Shine et al., 2017). These models generally use continuum-level approaches to capture mechanical degradation according to observations from macroscopic experiments (Bergström and Hayman, 2016; Hayman et al., 2014; Soares et al., 2010). While these approaches have provided reasonable predictions of mechanical behaviour, they offer little insight into role of physical properties on mechanical performance. Recently, micromechanical models of heterogeneous materials have emerged that have provided novel insight into the behaviour of polycrystalline metals (Dunne et al., 2007; Needleman and Tvergaard, 1993; Sweeney et al., 2013), composites (Vaughan and McCarthy, 2011) and ceramics

(Das et al., 2018). These approaches typically use the finite element method to apply macroscopically-equivalent loading (Ronan et al., 2014; Vaughan and McCarthy, 2010) to a representative volume element (RVE) of a material to enable micro- and macroscopic relations to be determined. While these have never been applied to semi-crystalline polymers, this physically-based modelling approach offers the exciting potential to better understand relationships between physical properties and mechanical performance during degradation.

In this study, a systematic evaluation of the physical, thermal and mechanical performance of medical-grade PLLA tubes undergoing thermally-accelerated degradation is presented. Samples are immersed in phosphate-buffered saline at 50°C for 112 days and measurements of mass loss, molecular weight, thermal properties, degree of crystallinity, elastic modulus, yield stress and ultimate stress/strain were evaluated at consecutive time points. A relationship between degradation rate and mechanical properties is analysed. This study also presents a computational micromechanics model that uses a Representative Volume Element of the PLLA microstructure to explore the relationship between molecular weight, percent crystallinity and the bulk mechanical properties.

2. Material and Methods

2.1. Material Specimens and Visual and Gravimetric Analysis

The material used in this study was medical-grade, semi-crystalline PLLA supplied in 1.5 mm diameter tubes that had been processed for vascular stenting applications. Samples for mechanical testing were laser-cut from expanded PLLA tubes in the shape of curved dog-bones, with the radius of half curvature measuring 1.5 mm (Figure 1). The gauge length of the samples was 5 mm and the sample thickness was 0.105 mm, which are therefore similar in dimension to typical stent struts of BRS devices. Samples used for thermal analysis and molecular weight measurement were from these same tubes, but the expansion step was omitted. The tubes were shredded, and appropriate weight masses were used for further experiments.

Visual examination of the samples was performed at each time point. Samples of 10 ± 0.5 mg were cut from the tubes and used to evaluate changes in mass over the course of degradation. At each time point, samples were removed from the solution, dried with a paper towel to remove surface moisture

and weighted in a wet condition to determine wet mass (VWR LA214, VWR International Ltd., West Chester, PA, USA). Next, samples were dried at 50°C overnight to remove moisture and their dry mass was measured. Water absorption was assessed based on the difference between wet and dry mass.

2.2. Accelerated degradation protocol

The *in vitro* accelerated degradation study followed protocols described by Weir et al. (N. A. Weir et al., 2004b) and ISO 13781:2017 (British Standards, 2017), taking place over a period of 112 days by immersing PLLA specimens in a phosphate-buffered saline (PBS) solution (Thermo Fisher Scientific, Waltham, MA, USA), and placing them in an oven that maintained an elevated temperature of 50°C (N. A. Weir et al., 2004b). The pH of the solution was maintained within pH 7.4 ± 0.2 (Orion Star A111 pH meter, Thermo Fisher Scientific, Waltham, MA, USA)(British Standards, 2017). Samples were removed from the solution at 10 consecutive time points to carry out physical, thermal and mechanical characterisation, whereby mass loss, molecular weight, thermal properties, degree of crystallinity, elastic modulus, yield stress and ultimate stress/strain were evaluated. Testing took place after 1, 7, 14, 21, 32, 49, 70, 91, and 112 days immersion. The accelerated degradation testing protocol of PLLA had been previously validated by real-time degradation (N. A. Weir et al., 2004a), with the elevated temperature of 50° being related back to service temperatures through the Arrhenius extrapolation assumption for thermally aged polymers (Wise et al., 1995):

$$k = Ae^{-Ea/RT} \tag{1}$$

where **k** is a rate constant; **A** is a constant; **Ea** is the activation energy, **R** is the universal gas constant (**R**= 8.314 J mol⁻¹ K⁻¹), and **T** is the temperature [K]. Based on degradation rate constants for accelerated and real-time degradation of an autocatalysed model (Pitt and Zhong-wei, 1987) used in a previous study, the in vitro degradation rate of PLLA was expected to be accelerated four-fold at 50°C compared to physiological temperatures of 37°C (N. A. Weir et al., 2004b).

2.3. Molecular Weight - Gel Permeation Chromatography

The number average (M_n), weight average (M_w) molecular weight and dispersity ($Đ = M_n/M_w$) of the samples were determined using Gel Permeation Chromatography (GPC) 3 detector system Malvern

PANalytical Viscotek TDAmax (Spectris, Egham, UK). Elution was done using Tetrahydrofuran (THF) at 1 ml/min and 35°C. At each time point, a 10 mg sample was removed from PBS solution, dried and dissolved in 2 ml chloroform ($CHCl_3$) to obtain a 5 mg/ml concentration solution. The GPC system was calibrated with polystyrene and results expressed as polystyrene equivalent molecular weight at each time point. The measurement was repeated three times for each timepoint.

2.4. Thermal Properties - Differential Scanning Calorimetry

Thermal behaviour of PLLA samples was measured using Differential Scanning Calorimetry (DSC). DSC experiments were performed at each time point (n=5) using Shimadzu DSC-60 system (Shimadzu Corp., Kyoto, Japan). All measurements began at room temperature, increasing to 300°C with a heating rate 10°C/min. Glass transition (T_g), melting point (T_m) and enthalpy of fusion were measured and the degree of crystallinity (X_c) of a sample was estimated relative to the enthalpy of fusion (ΔH_{melt}) of a 100% crystalline sample of PLLA reported to be 93 J/g (Fischer et al., 1973):

$$X_c = \frac{\Delta H_{melt}}{93} \times 100\% \qquad (3)$$

2.5. Spectroscopy Analysis

Raman spectroscopy measurements were performed in reflection mode with a confocal Raman microscope (Alpha 500, WITec Wissenschaftliche Instrumente und Technologie GmbH, Ulm, Germany) using 785 nm excitation. The detector grating used was 600 lines/mm, centred at 890 cm^{-1}. Spectra were collected using an Andor Ixus cooled charge coupled device (−60 °C). A 100x objective lens (NA 0.9) delivered the laser beam and collected the back-scattered light. Rayleigh scattering was blocked with the appropriate notch filter. The laser spot diameter was approximately 1 μm with a laser power of 0.05 mW (785 nm) used. The instrument calibration was verified using the maximum signal from a silicon standard at 520 cm^{-1} and spectral resolution was approximately 0.8 cm^{-1}. Cosmic ray reduction, background correction (shape correction), Savitzky-Golay smoothing (2 point, 2nd order) and spectrum averaging were carried out using WITec Project FIVE® software (WITec Wissenschaftliche Instrumente und Technologie GmbH, Ulm, Germany). Graphical analysis was performed using Origin® version 9.1 (OriginLab, Northampton, MA, USA). All spectra described are plotted relative to the excitation

wavelength. For each scan, 25 random points were taken over the sample surface and data were averaged over these 25 spectra.

FTIR spectra were carried out using the Varian 660-IR FT-R Spectrometer (Aligent Technologies, Santa Clara, CA, USA). Absorbance spectra were obtained by taking 16 scans per sample over the range 4000-500 cm^{-1}. Spectra were averaged over these 16 scans and background ratios were subtracted. Raman and FTIR spectra for PLLA at day 0, day 49 and day 91 were obtained. The bands observed in the spectra were analysed to examine differences between timepoints.

2.6. Scanning Electron Microscopy Imaging

Scanning Electron Microscopy (SEM) (S2600N Variable Pressure SEM, Hitachi, Tokyo, Japan) was carried out at several time points to examine fracture surfaces of PLLA samples post-mechanical testing. Samples were mounted on stages using carbon cement and sputter coated with gold under vacuum to make them conductive to electrons and examined using 5 kV voltage with magnifications ranging from x30 to x10,000.

2.7. Mechanical Characterisation

To evaluate temporal changes in mechanical properties, uniaxial tensile testing of the PLLA dog-bone specimens was carried out using a Zwick mechanical test machine with a 100N load cell (Zwick GmbH & Co., Ulm, Germany). Due to curved shape of the dog-bone specimens, a set of bespoke curved clamps were designed and manufactured (Riteway Engineering, Galway, Ireland) that securely gripped each specimen without introducing stress concentrations and/or or damage during clamping or testing (Figure 1). Following ISO 13781 (British Standards, 2017), uniaxial tensile tests were performed at each time point (n=3) on wet samples within 3 hours after removal from the solution at room temperature. Specimens were tested at a displacement rate of 10 mm/min, with extension and loading force recorded, which was used to calculate engineering stress and strain throughout the loading history based on undeformed specimen dimensions. The Young's modulus (E), ultimate stress (σ_{UTS}), ultimate strain (ε_u), and yield stress (σ_Y) were determined, with the latter calculated using standard regression slope method (British Standards, 2012). It should be noted that the dog-bone specimens became extremely brittle at late-stage time points (>day 70) and it was not possible to perform uniaxial tensile testing as specimens attained a slight curvature in their axial direction (Figure 3), which lead to fracture

when mounting in the clamps. As an alternative, nanoindentation testing was carried out to determine elastic modulus and hardness at several sample timepoints, with information on this included in the supplementary data.
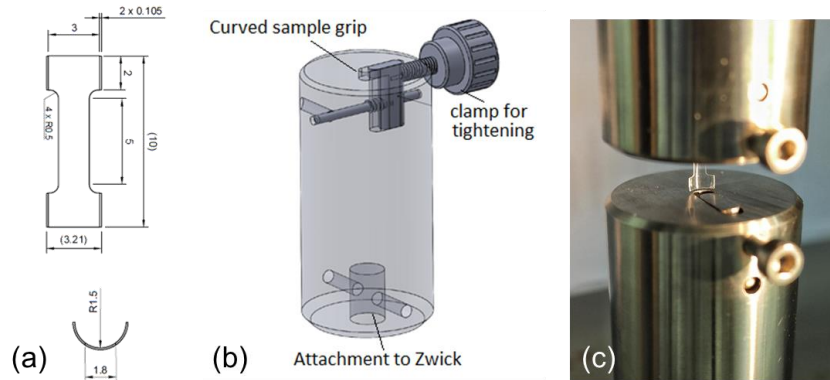
Figure 1 (a) Shape and dimensions of the samples used in the accelerated degradation study. (b) Dedicated clamps designed to grip curved shaped dog-bone samples. (c) Clamps with dog-bone sample being inserted.

2.8. Hydrolysis Kinetics

The hydrolytic degradation can be described by the chain end concentration which is directly related to number average molecular weight M_n. Therefore, degradation rate is often presented as molecular weight in function of time (Lyu and Untereker, 2009). Certain chain ends can be simultaneously products of one reaction and reactants in another, thus to precisely describe the product generation process of hydrolysis as the increase of chain ends concentration in time, the quantity of $1/M_n$ versus time is used (Lyu et al., 2007).

2.9. Computational Micromechanics Model

A micromechanical model of the semi-crystalline PLLA material was developed using a representative volume element (RVE) approach, which is shown schematically in Figure 2. Hexagonal regions were randomly assigned to be either amorphous or crystalline and a sensitivity study was performed to ensure that the RVE was statistically homogeneous (~1000 regions). For crystalline regions, each crystal was anisotropic and the orientation of each crystal in randomly assigned (i.e. the RVE is isotropic), with longitudinal ($E_{CL} = 7.14\ GPa$) and transverse ($E_{CT} = 4.14\ GPa$) moduli taken from the bounds reported for anisotropic PLA crystal aggregates (Lin et al., 2010). Amorphous regions were

isotropic and the modulus of the amorphous phase E_{am} assumed to vary with molecular weight, as collated by Gleadall (Gleadall, 2015) based on multiple studies and also observed in fully amorphous PLGA during degradation by Shirazi et al. (Shirazi et al., 2016):

$$E_{am} = E_{am0} + k_m \log_{10} \frac{M_n}{M_{n0}}, \quad [\frac{M_n}{M_{n0}} = \frac{M_n^{am}}{M_{n0}^{am}}] \tag{4}$$

where $k_m = 1400 MPa$ is an empirical constant, $E_{am0} = 1.83 GPa$ is the initial, undegraded modulus of the amorphous phase (Tsuji, 2002) and M_n and M_{n0} are the number-averaged molecular weight and its initial value. Thus, the experimentally-measured values of M_n and X_c reported in Table 1 were used as inputs to generate an RVE for each time point during degradation. Periodic boundary conditions were imposed and a uniaxial, nominal strain ($\varepsilon_{xx}^N = 1\%$) applied via displacement control in a non-linear, implicit finite element calculation (Abaqus 2019, Dassault Systèmes, RI, USA). The resulting reaction force was used to calculate a nominal stress σ_{xx}^N acting on the RVE and an effective modulus for the RVE is defined as the secant modulus at 1% strain:

$$\bar{E} = \left(\frac{\sigma_{xx}^N}{\varepsilon_{xx}^N} \right)_{\varepsilon_{xx}^N = 1\%} \tag{5}$$
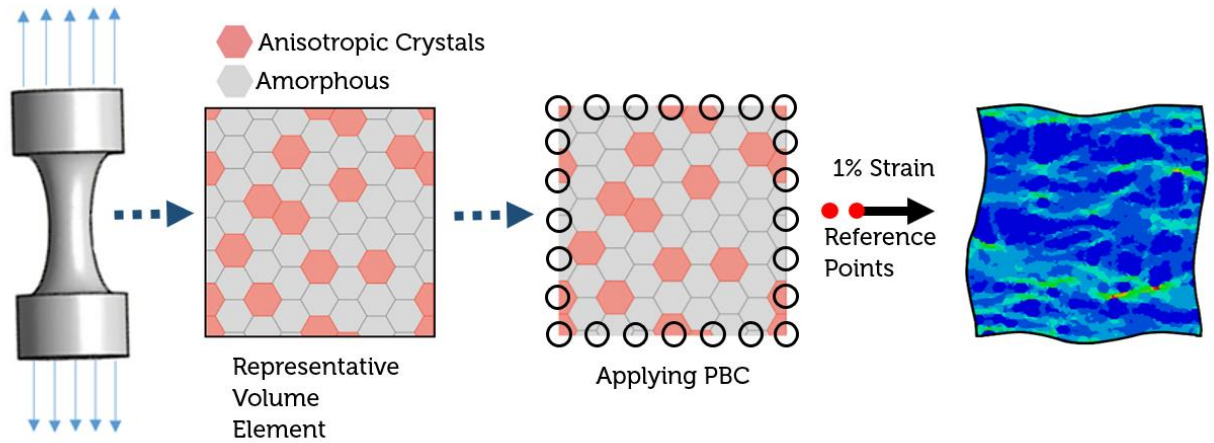
Figure 2: Micromechanical modelling of a semi-crystalline polymer using a representative volume element (RVE) approach.

3. Results

3.1. Visual and Gravimetric Analysis

Visual examination of the samples showed that the tubes, which were initially transparent, gradually turned translucent and opaque after day 49 (Figure 3a). Meanwhile, dog-bone samples remained transparent throughout the study, but displayed an increased curvature on their long-axis from day 70 of degradation (Figure 3b). Specimens became increasingly brittle, with handling becoming progressively difficult at later time-points. By day 112, several samples showed visible fractures and damage that was initiated by gentle handling.
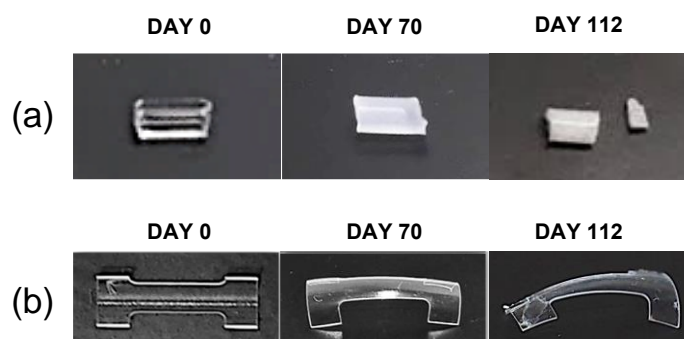
Figure 3: (a) Tubular samples used for mass change, GPC and DSC experiments changed from transparent to opaque and brittle with degradation. (b) Dog-bone samples used for tensile testing deforming during degradation.

There was no substantial mass loss observed over the period of 16 weeks (see Supplementary Material, Figure S2). Repeated measurements have shown no dry mass change during the time of the accelerated degradation monitored in the study. There was a constant average 0.7 mg decrease of mass between wet and dry samples which suggests that samples absorbed nearly 10% of their weight in water during immersion.

3.2. Solution pH Monitoring

The pH of the PBS solution in which the samples were immersed was regularly measured and has shown consistent decreases pointing at solution acidification possibly related to degradation (Rodrigues et al., 2016). The solution had to be changed on average every 3-4 weeks to maintain it within the range of pH 7.4 ± 0.2. Due to regular solution replacement, the analysis of acidification progress during the course of the whole study was not feasible.

3.3. Molecular Weight

The evolution of number (M_n) and weight (M_w) average molecular weight during the study are shown in Figure 4 and corresponding values provided in Table 1. The number average molecular weight of the PLLA samples at day 0 was measured as M_n = 97,650 ± 9,800 g/mol, and weight average molecular weight M_w = 218,640 ± 4,000 g/mol (dispersity Đ = 2.26 ± 0.19). There was an initial increase observed in both M_n and M_w on day 7 (M_n = 135,800 ± 7,400 g/mol, M_w = 239,000 ± 1,900 g/mol), followed by a steady decrease of almost 95% until day 112 (M_n = 7,430 ± 330 g/mol, M_w = 11,030 ± 140 g/mol) compared to day 7 (Figure 4). Dispersity on the other hand, decreased initially from 2.26 to 1.78 between days 0-14 after which it remained constant, increasing slightly to 1.95 on day 91, and dropping to 1.49 on day 112 (Table 1, Table S1).
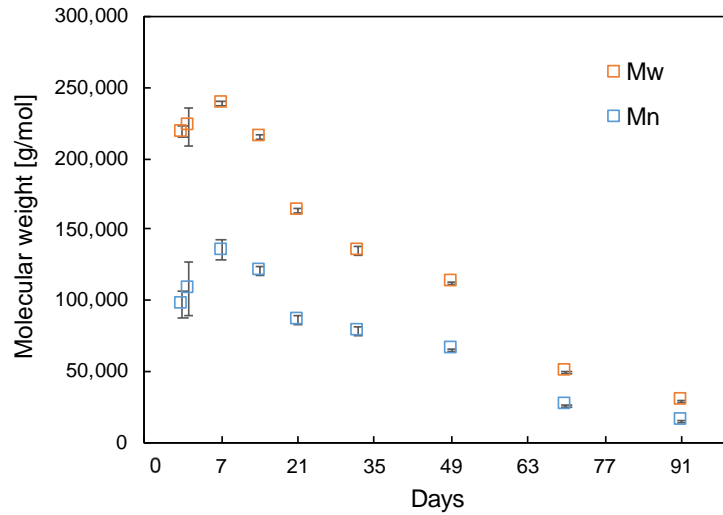
Figure 4 Evolution of number average molecular weight M_n and weight average molecular weight M_w over accelerated degradation period with error bars showing standard deviations.

Table 1: Experimental measurements and computational predictions of physical and mechanical properties.

Day	Experimental					Computational	
	M_w	M_n	Đ	X_c	E	E_{am}	$\bar{E}$
(accelerated)	(g/mol)	(g/mol)	( )	(%)	(GPa)	(GPa)	(GPa)
0(0)	218,638	97,647	2.26	38.59	2.258	1.830	2.91
1(4)	222,425	108,425	2.10	43.24	2.761	1.894	3.20
7(28)	238,970	135,765	1.76	39.45	2.418	2.030	3.16
14(56)	215,295	120,713	1.78	44.69	2.836	1.959	3.32
21(84)	163,421	86,012	1.90	49.05	2.654	1.753	3.29
32(128)	135,212	78,553	1.72	54.00	2.712	1.698	3.50
49(196)	112,897	65,086	1.73	57.77	2.643	1.583	3.56
70(280)	50,208	26,244	1.91	60.28	2.563	1.031	3.03
91(364)	30,028	15,369	1.95	67.30	-	0.706	3.11
112(448)	11,029	7,428	1.49	64.87	-	0.264	1.94

3.4. Thermal Properties

Figure 5a shows representative curves obtained from DSC testing at several time points, with the evolution in glass transition temperature (T_g), melting temperature and degree of crystallinity over the course of degradation shown in Figure 5b (Table S2). At day 0, the DSC curves show a first endothermic transition that is representative of a glass transition temperature (T_g) of a sample, which is followed by an exothermic peak of cold crystallisation. The most prominent endothermic peak represents the melting temperature (T_m). All of the peaks are present and clearly distinguishable on a DSC curve until day 32. On day 49, the cold crystallisation peak becomes indistinguishable, and the glass transition becomes less prominent, becoming only slightly visible on day 70. After day 91, the glass transition is no longer present and only the melting peak remains. No glass transition temperature change was observed in the course of the study. On the other hand, there was a decrease in melting point temperature (183°C on days 0-14 to 165°C on day 112) and almost two-fold increase in degree of crystallinity (38.6% before degradation to 65% on day 112).
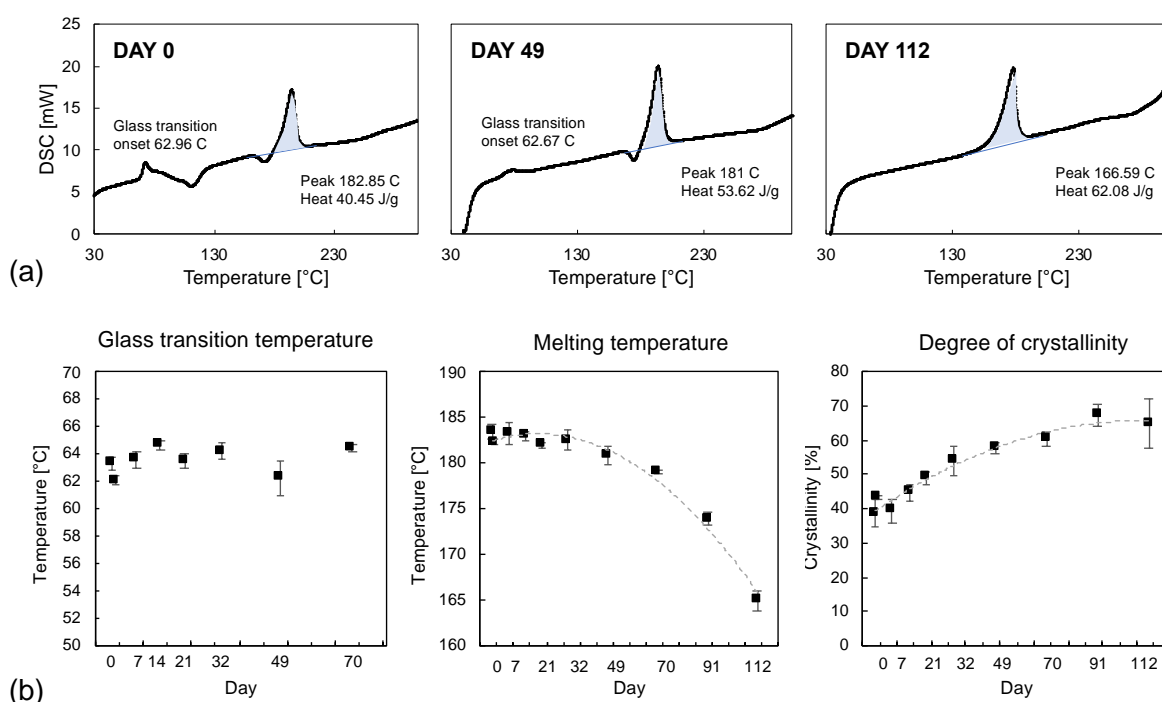
Figure 5 (a) DSC signal in PLLA samples before, after 49 days and 112 days of accelerated degradation. (b) Glass transition, melting point and degree of crystallinity evolution of PLLA samples during accelerated degradation.

3.5. Spectroscopy Analysis

The Raman and infrared spectra of the non-degraded (day 0) and degraded (up to day 91) PLLA polymers are shown in Figure 6. Assignments of vibrational infrared and Raman bands are explained based on the spectra presented and are summarised in **Error! Reference source not found.**.
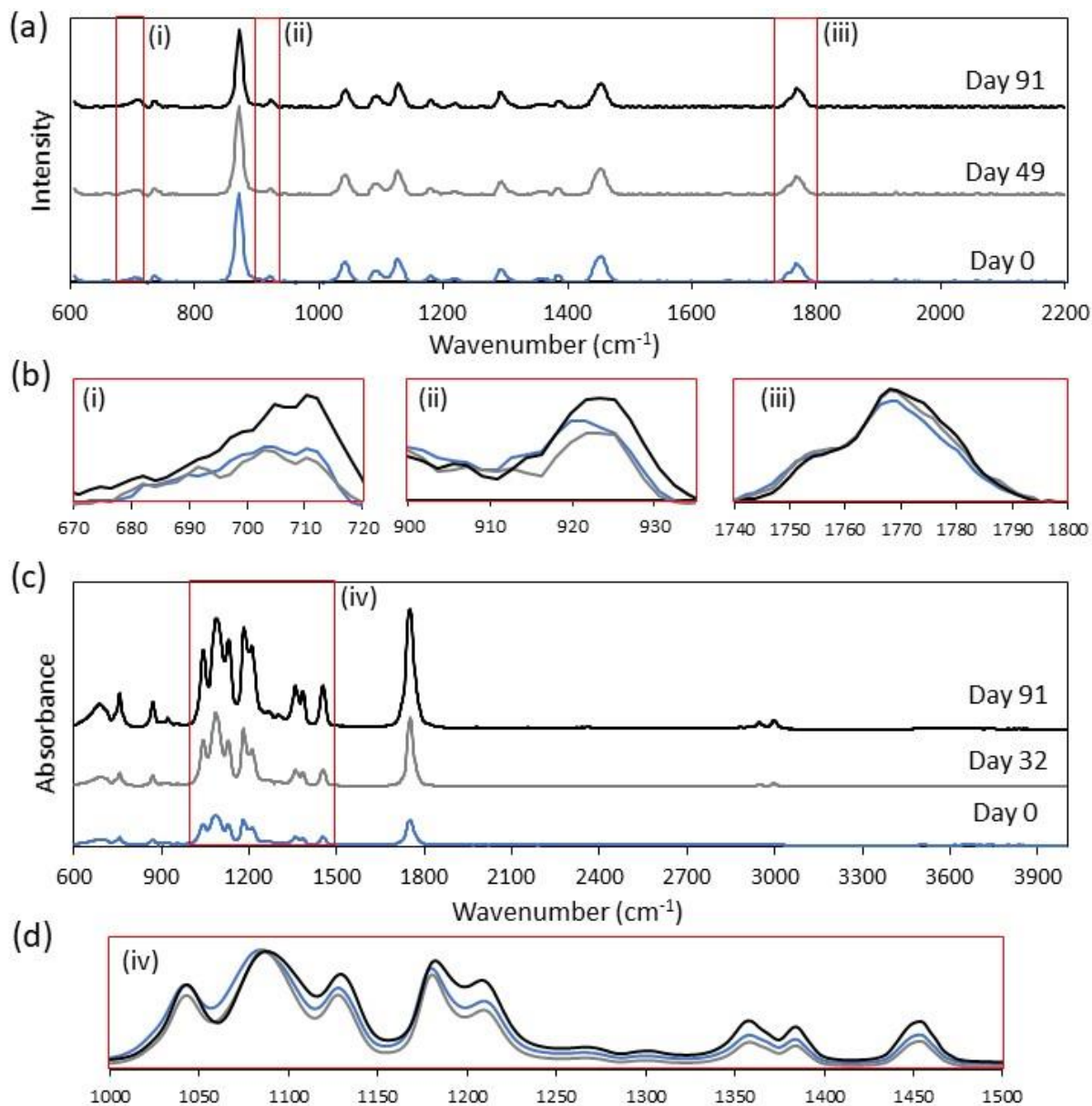
Figure 6 Raman spectra of PLLA samples from (a) 600 cm^{-1} to 2200 cm^{-1} (b) 670 cm^{-1} to 1800 cm^{-1} before, after 49 days and 91 days of accelerated degradation. Infrared spectra of PLLA samples from (c) 600 cm^{-1} to 4000 cm^{-1} (d) 1000 cm^{-1} to 1500 cm^{-1} before, after 32 days and 91 days of accelerated degradation.

For the Raman spectra, the band at 1452 cm^{-1} corresponds to the vibration of asymmetric bending of CH_3 in the lactic units of the polymer. It was observed that the intensity of this band was the least affected peak throughout the degradation process, therefore; to visualise the relative band intensity changes occurring over the hydrolysis time, the spectrum was normalised to prominent 1452 cm^{-1} peak.

14

Infrared spectra in the 1700-1800 cm^{-1} region assigned to the stretching modes of the carbonyl group ($C = O$). Splitting of the band centred on 1768 cm^{-1} is associated with the presence of crystalline phase in the PLLA polymer (Kister et al., 1995), as shown in Figure 6 (b). This indicates crystallinity of the polymer at day 0 and other degradation time points, which is consistent with the results obtained from DSC testing. The increase in the relative intensity of the peak centred on 1768 cm^{-1} over the hydrolysis time indicates a more crystalline phase of PLLA over the hydrolysis time; however, this change is not substantial. In addition to a splitting of the peak centred on 1768 cm^{-1}, the peaks at 923 cm^{-1} and 710 cm^{-1} correspond to the coupling of the $C - C$ backbone stretching with CH_3 rocking mode and torsion of the $C = O$ group, respectively, are associated with the crystalline phase (Vano-Herrera and Vogt, 2017), as shown in Figure 6 (b). The band at 873 cm^{-1} is the most intense peak and corresponds to the vibration of $C - COO$ stretching in the lactic units of the polymer.

The FTIR spectra present the common features of PLA polymers formed of lactic acid units. A clear peak at 1211-1184 cm^{-1} corresponds to the coupling of COC backbone asymmetric stretching with asymmetric rocking mode of the CH_3 group and the band observed at 1270 cm^{-1} assigned to CH bending, which is typical of PLLA polymer (Figure 6c). The absorption band at 923 cm^{-1} corresponds to stretching of $C - C$ and rocking of CH_3 band vibrations represent the crystalline structure of PLLA specimens; the change in the intensity of this band is not significant for different degradation timepoints. Most generally the relative intensity of all the bands across the full FTIR spectra do not show substantial changes over the course of degradation. However, a slight increase in the relative intensity of the peak centred on 1752 cm, which is assigned to the stretching of carbonyl group ($vC = O$), indicates a more crystalline phase of PLLA for later hydrolysis time. In the 1000-1150 cm^{-1} region, the bands appeared at 1127 cm^{-1}, 1087 cm^{-1}, and 1042 cm^{-1} correspond to the vibrations of the asymmetric rocking of CH_3, symmetric stretching of COC, and $C - CH_3$ stretching from the lactic acid units, respectively (Figure 6d). The FTIR spectra was normalised to prominent absorbance of the peak observed at 1087 cm^{-1} to visualise the relative band intensity changes occurring during the hydrolysis degradation. The results showed that the bands in this region seem more symmetric for the earlier degradation timepoints. The band observed at 1087 cm^{-1} also shifted slightly to the higher frequency by increasing the hydrolysis time.

3.6. SEM Analysis

Figure 7a and b show the surface of a sample obtained after rupture in tensile test before degradation and a fracture surface of a brittle sample resulting from handling after 112 days of accelerated degradation, respectively. In the non-degraded sample, a clean smooth surface with laminar structure along the failed edge and a lip characteristic for ductile type of fracture is observed. In contrast, a surface fracture of a sample after 112 days of accelerated degradation exhibited cracks and sharp edges typical of a brittle fracture surface.
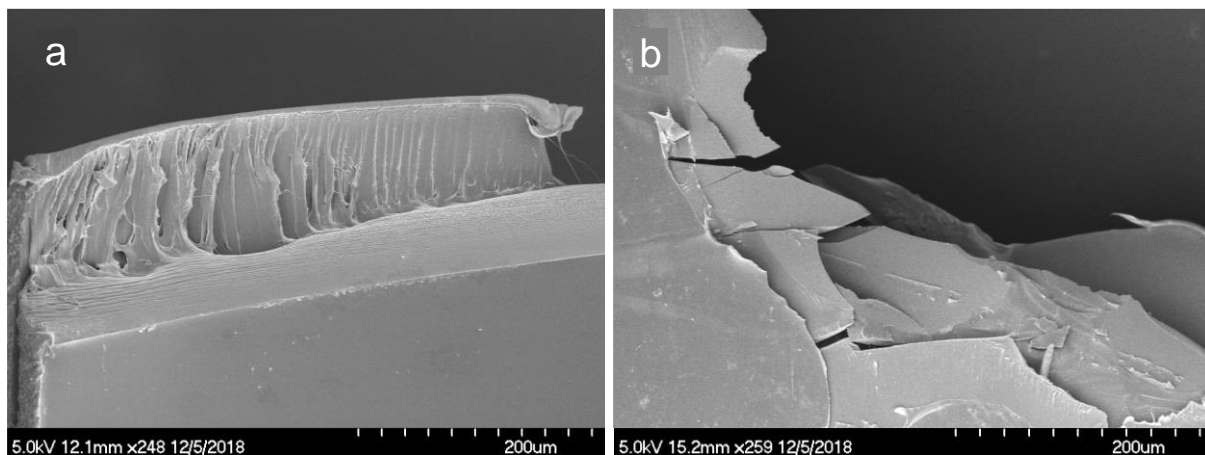
Figure 7 SEM images of dog-bone samples damage surfaces obtained with 5kV and magnification approximately x250. (a) Failure surface of a dog-bone sample before degradation exhibiting ductile failure in tensile test. (b) Failure surface of a dog-bone sample after 112 days of degradation showing brittle fracture resulting from gentle handling.

3.7. Mechanical Properties

Mechanical tensile tests were performed up to day 70 of the accelerated degradation. After this time point, PLLA dog-bone samples exhibited increased brittleness and curvature induced by the degradation process. This resulted in specimens fracturing during, or even prior, to clamping in the special-purpose clamping grips. Figure 8a shows representative stress-strain curves from several time points (for all average stress-strain curves see Figure S3). It is notable that prior to day 70, the stress-strain behaviour is characteristic of a ductile polymer behaviour, with an initial linear increase in stress, followed by a peak stress and a long plastic plateau. Beyond day 70, a distinct change in mechanical behaviour was observed, with samples becoming more brittle and fracturing almost immediately post-yield, exhibiting only small amounts of plastic deformation. At day 0 (non-degraded samples), material properties were evaluated as Young's modulus $E = 2.26 \pm 0.26$ GPa, ultimate engineering stress $\sigma_{UTS} = 115.2 \pm 2.5$ MPa, ultimate engineering strain $\varepsilon_{UTS} = 0.69 \pm 0.02$, and yield stress and strain respectively

$\sigma_Y = 84.6 \pm 2.9$ MPa, $\varepsilon_Y = 0.047 \pm 0.013$ (Table S3). After degradation, the ultimate strain (ε_{UTS}) showed the most significant change (77% decrease between days 0 and 70) (Figure 8c) with a smaller decrease observed for ultimate stress (14% decrease) (Figure 8b). Yield stress and yield strain were observed to decrease only slightly. Interestingly, there was no change in Young's modulus observed following degradation (Figure 8d). This was also true for modulus measured with nanoindentation, which have also shown that the modulus was unchanged up to day 91 (see Supplementary Material, Section 2.4.2).
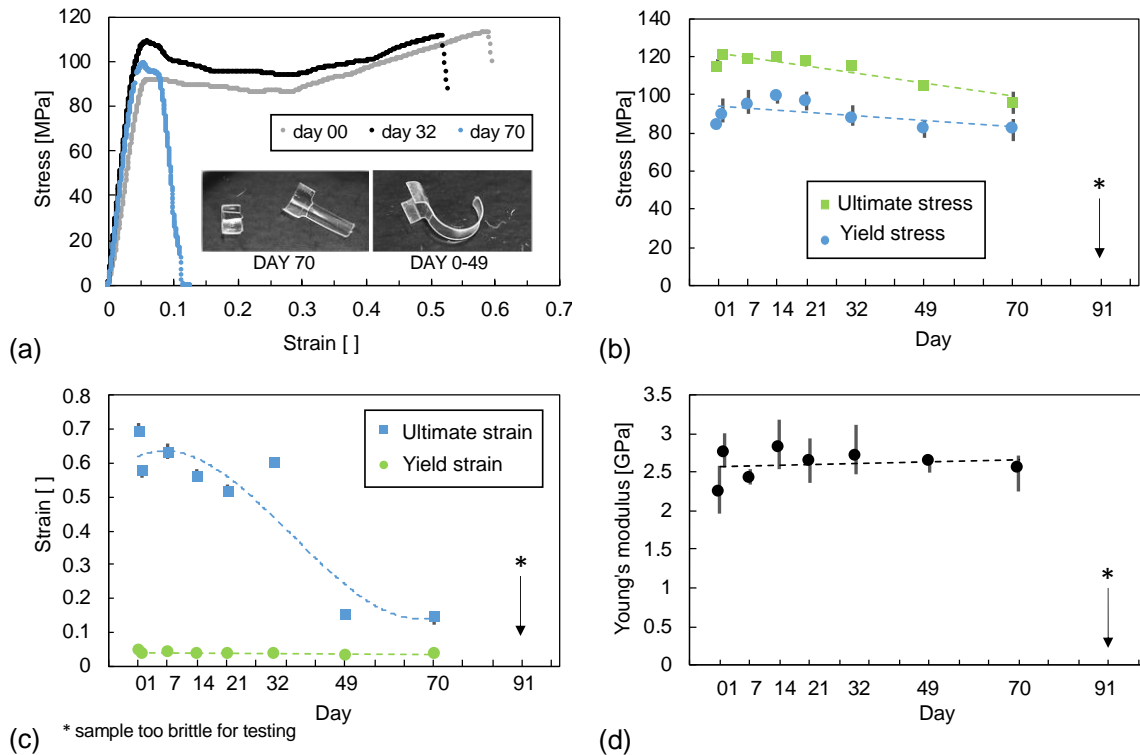
Figure 8 Mechanical properties of PLLA dog-bone samples changing with degradation; (a) Representative stress-strain curves for PLLA samples before accelerated degradation, after 32 days and 70 days. Inset images show dog-bone samples after failure in tensile test. (b) Averaged tensile yield strength and ultimate strength of the dog-bone samples. (c) Averaged tensile yield strain and ultimate tensile strain. (e) Averaged tensile Young's modulus of the dog-bone samples. Plots b-d show average values and grey bars representing range between minimum and maximum value.

3.8. Hydrolysis Kinetics

Degradation rate $1/M_n$ versus time (Figure 9) has shown piecewise linear trend with two distinct regions with different slopes. A rapid acceleration in degradation was observed around day 52 which can be translated to day 208 of degradation in real time. This rate increase followed directly the rapid decrease in strain to failure (Figure 8c) observed on day 49 (day 196 in real time degradation).
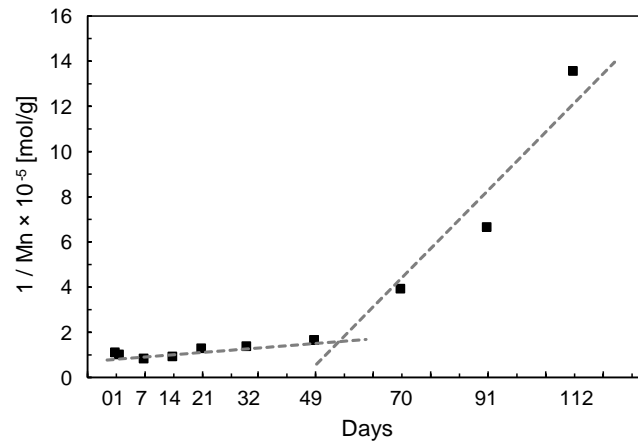
Figure 9 Degradation rate *1/Mn* versus time showing distinct rate increase on day 52 of accelerated degradation of PLLA.

3.9. Computational Micromechanics

For each experimentally reported value of M_n and X_c, a simulation was performed (with the corresponding fraction of crystalline regions and appropriate E_{am}) to determine the homogenised modulus, $\bar{E}$. The predicted modulus values are reported in Table 1 and shown in Figure 10b, where there is good agreement with the experimentally-measured modulus, with the model predicting similar increases in $\bar{E}$ in initial phase of degradation (up to day 49). The simulations also predicted modulus values for the cases where the experimental samples were too brittle to test, with these results supporting the hypothesis that a substantial reduction in mechanical integrity had occurred at day 112. Figure 10a shows the stress distribution (both the stress in the loaded direction σ_{11} and the tensile equivalent stress σ_{vm} at three selected time points, days 0 ,70, and 112. During degradation, as the crystallinity increases from 39% at day 0 to 65% at day 112, the stress becomes more localised, with stress concentrations forming between closely-neighbouring crystals.
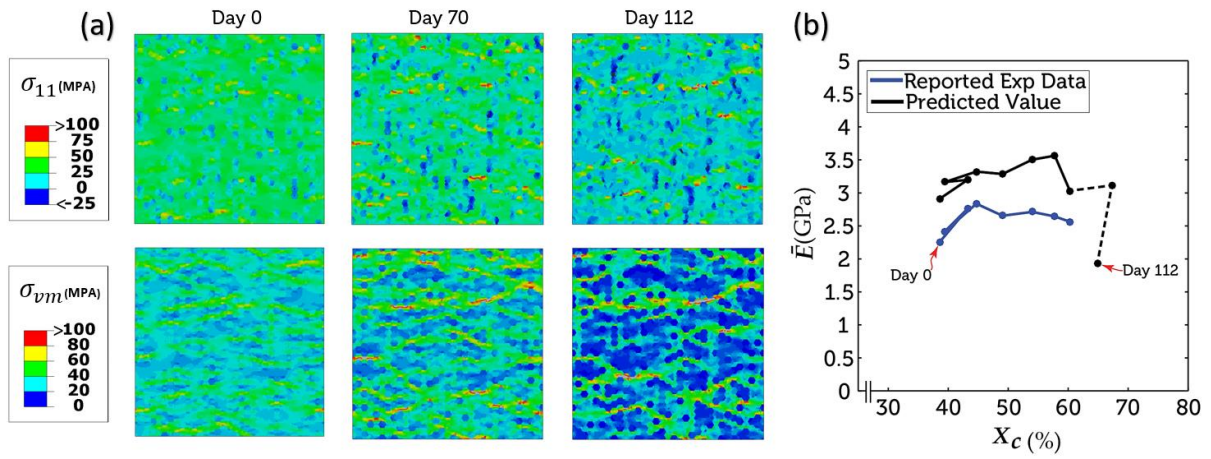
Figure 10 Results from micromechanical simulations. (a) σ_{11} and σ_{vm} distribution at three selected time points. (b) Model predictions (black) compared to experimental data.

4. Discussion

This study presents a comprehensive evaluation of the physical, thermal and mechanical behaviour of medical-grade PLLA undergoing thermally-accelerated degradation. In the first phase (<day 30), samples showed a consistent reduction in molecular weight, with only minor changes in mechanical properties. In the second phase (day 35-70), despite further reductions in molecular weight, samples maintained their elastic modulus, yield and tensile strength, however showed a substantial reduction in tensile failure strain. In the third phase (day 70 - 112), samples became too brittle to test indicating substantial deterioration of their load-bearing capacity. Across all phases, there was a consistent increase in degree of crystallinity, decrease in melt temperature, minor changes in glass transition temperature and no measurable mass loss. Loss of tensile failure strain was coincident with rapid increase in degradation rate. This study also presented a computational micromechanics framework that provided novel insight into the relationship between physical and mechanical behaviour over the course of degradation. Notably, it was demonstrated that the modulus of a semi-crystalline polymer undergoing degradation can be maintained, despite a reducing molecular weight through compensatory increases in percent crystallinity.

The results of mechanical tests have provided novel insight into the precise mechanism of degradation within this PLLA material, with its load-bearing ability unchanged after 49 days, despite a 50% reduction in molecular weight at this point. Assuming a four-fold acceleration of the degradation process at 50°C, this indicates that the mechanical integrity of a PLLA-based scaffold would be maintained for >6 months at a physiological temperature of 37°C. While this suggests that the medical-grade PLLA in the current study has been processed to maximise its load-bearing capacity for BRS applications, it is notable that the material becomes highly brittle at later time points. This ductile to brittle transition, which was clearly observed when fracture surfaces were examined using SEM imaging, could have implications for fracture and breakage of stent struts in BRS devices beyond 6 months after implantation. Interestingly, the drastic reduction in post-yield ductility was associated with rapid increase in degradation rate. We speculate that monitoring and more precise control over degradation rate of the material could reduce the risk of sudden strut discontinuity in BRS leading to late stage complications. Degradation rate $1/M_n$ might be a potential indicator of mechanical performance of a stent.

Moreover, increase in brittleness was associated with consistent increases in percentage crystallinity of the polymer over the course of degradation. The increased crystallinity observed here implies a reduction in the proportion of (or a preferential degradation of) the amorphous regions. This increased crystallinity was observed through both DSC testing and FTIR spectroscopy, with the latter showing more symmetric bands in the 1000-1150 cm^{-1} region for the earlier degradation timepoints and the band at 1087 cm^{-1} shifting slightly to the higher frequency as hydrolysis progresses (Kister et al., 1998). Here, the hydrolysis process leads to a reduction in polymer chain lengths in the amorphous phase (e.g. reduced molecular weight), increasing mobility and enabling re-crystallisation through scission-induced realignment of these shorter polymer chains, resulting in a nett increase in the degree of crystallinity, Xc and a corresponding decrease in the proportion of amorphous phase present. While the crystalline phase contributes to polymer strength and stiffness (Liu et al., 2014) (which remain largely unchanged), the amorphous phase is generally responsible for a ductility to the material as tangled polymer chains slide over one another and disentangle, allowing the material to plastically deform. This is likely a reason for the increased brittleness observed at later time points. On the contrary, other thermal-accelerated degradation study of non-medical grade PLLA (N. A. Weir et al., 2004b) have shown that elastic mechanical properties deteriorate proportionally with molecular weight.

This study also presented a computational micromechanics framework that provided novel insight into the relationship between physical and mechanical behaviour over the course of degradation. A large proportion of previous models of polymer degradation have assumed an empirical relationship between the Young's modulus and molecular weight (Shirazi et al., 2016; Wang et al., 2010). While such models may be appropriate for amorphous materials (Shirazi et al., 2016; Wang et al., 2010), our experimental results, as well as others (Dreher et al., 2016; Tsuji, 1995; Tsuji and Ikada, 1998), clearly show that molecular weight alone does not govern mechanical response of semi-crystalline materials. Our micromechanical model clearly demonstrates that the crystal phase heavily influences the mechanical response and elucidates that there are two competing mechanisms affecting the effective modulus during degradation. Firstly, increases in crystallinity tend to increase the modulus due to a larger fraction of this stiffer material phase (E_{CL}), while decreases in molecular weight of the amorphous phase lead to a decrease in modulus in that phase (E_{am}), lowering the overall effective modulus. However, both processes proceed simultaneously and largely negate one another, which implies that elastic modulus

can remain unchanged, despite substantial changes in properties of the amorphous phase (E_{am}) and percentage crystallinity (X_c) This supports the experimentally-observed increases in X_c (due to recrystallization) and decreases in M_w (due to preferential degradation of amorphous regions) and minimal changes in E.

There are certain limitations within this study that should be acknowledged. Firstly, the study uses thermally accelerated degradation to model the physiological environment of implanted BRS, with the total time of the study translating to 448 days in the accelerated timeframe. This protocol is based on thermally-accelerated studies by Weir *et al.* (N. A. Weir et al., 2004b), who demonstrated that the mechanisms of degradation remain the same, particularly when carried out below T_g. Importantly, the glass transition temperature of the PLLA material remains higher (63.3°C) than the immersed temperature for the duration of the study and it is therefore expected that the degradation kinetics are largely similar to those at physiological temperatures. Secondly, the computational micromechanical model predicts values of modulus that are lower than those reported. While this discrepancy could be a result of the uniformly shaped crystal regions and the assumption of a two-dimensional RVE, it is important to note that this model captures similar trends to those observed experimentally. Of course, this model only considers the micromechanical response of semi-crystalline PLLA in the elastic regime, but still provides novel insight into the local microstructural stress distribution under loading. In particular, increased stress concentrations are predicted at later time degradation time points, which occur within and immediately adjacent to the stiffer crystal regions. Interestingly, these stress concentrations form approximately linear patterns, suggesting that a cascade of local failures could result micro-crack formation at these locations at later time-points, which could explain the experimental observations of reduced ductility in PLLA.

5. Conclusions

This study presented a material-level evaluation of physical, thermal and mechanical properties for medical-grade PLLA samples undergoing thermally accelerated degradation. In combination with a computational micromechanics framework, our results demonstrated that the load-bearing capacity of this semi-crystalline polymer undergoing degradation is maintained, despite a reducing molecular weight, through compensatory increases in percent crystallinity. However, the higher degree of crystallinaity led to increased brittleness of PLLA samples followed by rapid degration rate increase, which could have important implications for fracture behaviour of implanted stents.

Acknowledgements

References

Antheunis, H., van der Meer, J.-C., de Geus, M., Kingma, W., Koning, C.E., 2009. Improved Mathematical Model for the Hydrolytic Degradation of Aliphatic Polyesters. Macromolecules 42, 2462–2471. https://doi.org/10.1021/ma802222m

Bartkowiak-Jowsa, M., Będziński, R., Kozłowska, A., Filipiak, J., Pezowicz, C., 2013. Mechanical, rheological, fatigue, and degradation behavior of PLLA, PGLA and PDGLA as materials for vascular implants. Meccanica 48, 721–731. https://doi.org/10.1007/s11012-012-9626-2

Bergström, J.S., Hayman, D., 2016. An Overview of Mechanical Properties and Material Modeling of Polylactide (PLA) for Medical Applications. Ann. Biomed. Eng. 44, 330–340. https://doi.org/10.1007/s10439-015-1455-8

British Standards, 2017. BS ISO 13781:2017 Implants for surgery — Homopolymers, copolymers and blends on poly(lactide) — In vitro degradation testing.

British Standards, 2012. BSI Standards Publication Plastics — Determination of tensile properties Part 1 : General principles, 527-1.

Cassese, S., Byrne, R.A., Ndrepepa, G., Kufner, S., Wiebe, J., Repp, J., Schunkert, H., Fusaro, M., Kimura, T., Kastrati, A., 2016. Everolimus-eluting bioresorbable vascular scaffolds versus everolimus-eluting metallic stents: A meta-analysis of randomised controlled trials. Lancet 387, 537–544. https://doi.org/10.1016/S0140-6736(15)00979-4

Das, S., Ronan, W., Wadley, H.N.G., Deshpande, V.S., 2018. Penetration of confined ceramics targets. Extrem. Mech. Lett. 18, 45–57. https://doi.org/10.1016/j.eml.2017.11.001

Dreher, M.L., Nagaraja, S., Batchelor, B., 2016. Effects of fatigue on the chemical and mechanical degradation of model stent sub-units. J. Mech. Behav. Biomed. Mater. 59, 139–145. https://doi.org/10.1016/j.jmbbm.2015.12.020

Dunne, F.P.E., Rugg, D., Walker, A., 2007. Lengthscale-dependent, elastically anisotropic, physically-based hcp crystal plasticity: Application to cold-dwell fatigue in Ti alloys. Int. J. Plast. 23, 1061–1083. https://doi.org/10.1016/j.ijplas.2006.10.013

Farrar, D.F., Gillson, R.K., 2002. Hydrolytic degradation of polyglyconate B: The relationship between degradation time, strength and molecular weight. Biomaterials 23, 3905–3912. https://doi.org/10.1016/S0142-9612(02)00140-0

Fischer, E.W., Sterzel, H.J., Wegner, G., 1973. Investigation of the structure of solution grown crystals of lactide copolymers by means of chemical reactions. Kolloid-Zeitschrift Zeitschrift für Polym. 251, 980–990. https://doi.org/10.1007/BF01498927

Gleadall, A., 2015. Mechanical properties of biodegradable polymers for medical applications, in: Modelling Degradation of Bioresorbable Polymeric Medical Devices. Elsevier Ltd, pp. 163–199. https://doi.org/10.1533/9781782420255.2.163

Gonzalo, N., Gonzalo, N., Macaya, C., 2012. Absorbable stent: focus on clinical applications and benefits. Vasc. Health Risk Manag. 125. https://doi.org/10.2147/VHRM.S22551

Grabow, N., Bünger, C.M., Schultze, C., Schmohl, K., Martin, D.P., Williams, S.F., Sternberg, K., Schmitz, K.-P., 2007. A Biodegradable Slotted Tube Stent Based on Poly(l-lactide) and Poly(4-hydroxybutyrate) for Rapid Balloon-Expansion. Ann. Biomed. Eng. 35, 2031–2038. https://doi.org/10.1007/s10439-007-9376-9

Grabow, N., Schlun, M., Sternberg, K., Hakansson, N., Kramer, S., Schmitz, K.P., 2005. Mechanical properties of laser cut poly(L-lactide) micro-specimens: Implications for stent design, manufacture, and sterilization. J. Biomech. Eng. 127, 25–31. https://doi.org/10.1115/1.1835349

Hayman, D., Bergerson, C., Miller, S., Moreno, M., Moore, J.E., 2014. The Effect of Static and Dynamic Loading on Degradation of PLLA Stent Fibers. J. Biomech. Eng. 136. https://doi.org/10.1115/1.4027614

Kimble, L.D., Bhattacharyya, D., 2015. In Vitro Degradation Effects on Strength, Stiffness, and Creep of PLLA/PBS: A Potential Stent Material. Int. J. Polym. Mater. Polym. Biomater. 64, 299–310. https://doi.org/10.1080/00914037.2014.945203

Kister, G., Cassanas, G., Vert, M., 1998. Effects of morphology, conformation and configuration on the IR and Raman spectra of various poly(lactic acid)s. Polymer (Guildf). 39, 267–273. https://doi.org/10.1016/S0032-3861(97)00229-2

Kister, G., Cassanas, G., Vert, M., Pauvert, B., Térol, A., 1995. Vibrational analysis of poly(L-lactic acid). J. Raman Spectrosc. 26, 307–311. https://doi.org/10.1002/jrs.1250260409

Kraak, R.P., Hassell, M.E.C.J., Grundeken, M.J., Koch, K.T., Henriques, J.P.S., Piek, J.J., Baan, J., Vis, M.M., Arkenbout, E.K., Tijssen, J.G.P., de Winter, R.J., Wykrzykowska, J.J., 2015. Initial experience and clinical evaluation of the Absorb bioresorbable vascular scaffold (BVS) in real-world practice: the AMC Single Centre Real World PCI Registry. EuroIntervention 10, 1160–1168. https://doi.org/10.4244/EIJY14M08_08

Lin, T., Liu, X.-Y., He, C., 2010. Ab Initio Elasticity of Poly(lactic acid) Crystals. J. Phys. Chem. B 114, 3133–3139. https://doi.org/10.1021/jp911198p

Lipinski, M.J., Escarcega, R.O., Baker, N.C., Benn, H.A., Gaglia, M.A., Torguson, R., Waksman, R., 2016. Scaffold Thrombosis after Percutaneous Coronary Intervention with ABSORB Bioresorbable Vascular Scaffold A Systematic Review and Meta-Analysis. JACC Cardiovasc. Interv. 9, 12–24. https://doi.org/10.1016/j.jcin.2015.09.024

Liu, G., Zhang, X., Wang, D., 2014. Tailoring crystallization: Towards high-performance poly (lactic acid). Adv. Mater. 26, 6905–6911. https://doi.org/10.1002/adma.201305413

Luo, Q., Liu, X., Li, Z., Huang, C., Zhang, W., Meng, J., Chang, Z., Hua, Z., 2014. Degradation Model of Bioabsorbable Cardiovascular Stents. PLoS One 9, e110278. https://doi.org/10.1371/journal.pone.0110278

Lyu, S.P., Schley, J., Loy, B., Lind, D., Hobot, C., Sparer, R., Untereker, D., 2007. Kinetics and time-temperature equivalence of polymer degradation. Biomacromolecules 8, 2301–2310. https://doi.org/10.1021/bm070313n

Lyu, S.P., Untereker, D., 2009. Degradability of Polymers for Implantable Biomedical Devices. Int. J. Mol. Sci. https://doi.org/10.3390/ijms10094033

Lyu, Schley, J., Loy, B., Lind, D., Hobot, C., Sparer, R., Untereker, D., 2007. Kinetics and Time−Temperature Equivalence of Polymer Degradation. Biomacromolecules 8, 2301–2310. https://doi.org/10.1021/bm070313n

Needleman, A., Tvergaard, V., 1993. Comparison of crystal plasticity and isotropic hardening predictions for metal-matrix composites. J. Appl. Mech. Trans. ASME 60, 70–76. https://doi.org/10.1115/1.2900781

Nuutinen, J.-P., Clerc, C., Reinikainen, R., Törmälä, P., 2003. Mechanical properties and in vitro degradation of bioabsorbable self-expanding braided stents. J. Biomater. Sci. Polym. Ed. 14, 255–266. https://doi.org/10.1163/156856203763572707

Patel, A., Nazif, T., Stone, G.W., Ali, Z.A., 2017. Intraluminal bioresorbable vascular scaffold dismantling with aneurysm formation leading to very late thrombosis. Catheter. Cardiovasc. Interv. 89, 876–879. https://doi.org/10.1002/ccd.26913

Pitt, C.G., Zhong-wei, G., 1987. Modification of the rates of chain cleavage of poly(ϵ-caprolactone) and related polyesters in the solid state. J. Control. Release 4, 283–292. https://doi.org/10.1016/0168-3659(87)90020-4

Qiu, T., He, R., Abunassar, C., Hossainy, S., Zhao, L.G., 2018. Effect of two-year degradation on mechanical interaction between a bioresorbable scaffold and blood vessel. J. Mech. Behav. Biomed. Mater. 78, 254–265. https://doi.org/10.1016/j.jmbbm.2017.11.031

Rodrigues, N., Benning, M., Ferreira, A.M., Dixon, L., Dalgarno, K., 2016. Manufacture and Characterisation of Porous PLA Scaffolds. Procedia CIRP 49, 33–38. https://doi.org/10.1016/j.procir.2015.07.025

Ronan, W., Deshpande, V.S., McMeeking, R.M., McGarry, J.P., 2014. Cellular contractility and substrate elasticity: A numerical investigation of the actin cytoskeleton and cell adhesion. Biomech. Model. Mechanobiol. 13, 417–435. https://doi.org/10.1007/s10237-013-0506-z

Serruys, P.W., Chevalier, B., Sotomi, Y., Cequier, A., Carrié, D., Piek, J.J., Van Boven, A.J., Dominici, M., Dudek, D., McClean, D., Helqvist, S., Haude, M., Reith, S., de Sousa Almeida, M., Campo, G., Iñiguez, A., Sabaté, M., Windecker, S., Onuma, Y., 2016. Comparison of an everolimus-eluting bioresorbable scaffold with an everolimus-eluting metallic stent for the treatment of coronary artery stenosis (ABSORB II): a 3 year, randomised, controlled, single-blind, multicentre clinical trial. Lancet 388, 2479–2491. https://doi.org/10.1016/S0140-6736(16)32050-5

Shine, R., Shirazi, R.N., Ronan, W., Sweeney, C.A., Kelly, N., Rochev, Y.A., McHugh, P.E., 2017. Modeling of biodegradable polyesters with applications to coronary stents. J. Med. Devices, Trans. ASME 11, 1–12. https://doi.org/10.1115/1.4035723

Shirazi, R.N., Ronan, W., Rochev, Y., McHugh, P., 2016. Modelling the degradation and elastic properties of poly(lactic-co-glycolic acid) films and regular open-cell tissue engineering scaffolds. J. Mech. Behav. Biomed. Mater. 54, 48–59. https://doi.org/10.1016/j.jmbbm.2015.08.030

Soares, J.S., Moore, J.E., Rajagopal, K.R., 2008. Constitutive Framework for Biodegradable Polymers with Applications to Biodegradable Stents. ASAIO J. 54, 295–301. https://doi.org/10.1097/MAT.0b013e31816ba55a

Soares, J.S., Rajagopal, K.R., Moore, J.E., 2010. Deformation-induced hydrolysis of a degradable polymeric cylindrical annulus. Biomech. Model. Mechanobiol. 9, 177–186. https://doi.org/10.1007/s10237-009-0168-z

Sorrentino, S., Giustino, G., Mehran, R., Kini, A.S., Sharma, S.K., Faggioni, M., Farhan, S., Vogel, B., Indolfi, C., Dangas, G.D., 2017. Everolimus-Eluting Bioresorbable Scaffolds Versus Everolimus-Eluting Metallic Stents. J. Am. Coll. Cardiol. 69, 3055–3066. https://doi.org/10.1016/j.jacc.2017.04.011

Stone, G.W., Granada, J.F., 2015. Very Late Thrombosis After Bioresorbable Scaffolds. J. Am. Coll. Cardiol. 66, 1915–1917. https://doi.org/10.1016/j.jacc.2015.08.863

Sweeney, C.A., Vorster, W., Leen, S.B., Sakurada, E., McHugh, P.E., Dunne, F.P.E., 2013. The role of elastic anisotropy, length scale and crystallographic slip in fatigue crack nucleation. J. Mech. Phys. Solids 61, 1224–1240. https://doi.org/10.1016/j.jmps.2013.01.001

Tsuji, H., 2002. Autocatalytic hydrolysis of amorphous-made polylactides: Effects of L-lactide content, tacticity, and enantiomeric polymer blending. Polymer (Guildf). 43, 1789–1796. https://doi.org/10.1016/S0032-3861(01)00752-2

Tsuji, H., 1995. Properties and morphologies of poly(l-lactide): 1. Annealing condition effects on properties and morphologies of poly(l-lactide). Polymer (Guildf). 36, 2709–2716. https://doi.org/10.1016/0032-3861(95)93647-5

Tsuji, H., Ikada, Y., 2000. Properties and morphology of poly(l -lactide) 4. Effects of structural parameters on long-term hydrolysis of poly(l -lactide) in phosphate-buffered solution. Polym. Degrad. Stab. 67, 179–189. https://doi.org/10.1016/S0141-3910(99)00111-1

Tsuji, H., Ikada, Y., 1998. Properties and morphology of poly(L-lactide). II. Hydrolysis in alkaline solution. J. Polym. Sci. Part A Polym. Chem. 36, 59–66. https://doi.org/10.1002/(SICI)1099-0518(19980115)36:1<59::AID-POLA9>3.0.CO;2-X

Vano-Herrera, K., Vogt, C., 2017. Degradation of poly(L -lactic acid) coating on permanent coronary metal stent investigated ex vivo by micro Raman spectroscopy. J. Raman Spectrosc. 48, 711–719. https://doi.org/10.1002/jrs.5111

Vaughan, T.J., McCarthy, C.T., 2011. Micromechanical modelling of the transverse damage behaviour in fibre reinforced composites. Compos. Sci. Technol. 71, 388–396. https://doi.org/10.1016/j.compscitech.2010.12.006

Vaughan, T.J., McCarthy, C.T., 2010. A combined experimental-numerical approach for generating statistically equivalent fibre distributions for high strength laminated composite materials. Compos. Sci. Technol. 70, 291–297. https://doi.org/10.1016/j.compscitech.2009.10.020

Venkatraman, S., Poh, T.L., Vinalia, T., Mak, K.H., Boey, F., 2003. Collapse pressures of biodegradable stents. Biomaterials 24, 2105–2111. https://doi.org/10.1016/S0142-9612(02)00640-3

Wang, Y., Han, X., Pan, J., Sinka, C., 2010. An entropy spring model for the Young's modulus change of biodegradable polymers during biodegradation. J. Mech. Behav. Biomed. Mater. 3, 14–21. https://doi.org/10.1016/j.jmbbm.2009.02.003

Wang, Y., Pan, J., Han, X., Sinka, C., Ding, L., 2008a. A phenomenological model for the degradation of biodegradable polymers. Biomaterials 29, 3393–3401. https://doi.org/10.1016/j.biomaterials.2008.04.042

Wang, Y., Pan, J., Han, X., Sinka, C., Ding, L., 2008b. A phenomenological model for the degradation of biodegradable polymers. Biomaterials 29, 3393–3401. https://doi.org/10.1016/j.biomaterials.2008.04.042

Weir, N.., Buchanan, F.., Orr, J.., Farrar, D.., Boyd, A., 2004. Processing, annealing and sterilisation of poly-l-lactide. Biomaterials 25, 3939–3949. https://doi.org/10.1016/j.biomaterials.2003.10.076

Weir, N.A., Buchanan, F.J., Orr, J.F., Dickson, G.R., 2004a. Degradation of poly-L-lactide. Part 1: in vitro and in vivo physiological temperature degradation. Proc. Inst. Mech. Eng. Part H J. Eng. Med. 218, 307–319. https://doi.org/10.1243/0954411041932782

Weir, N.A., Buchanan, F.J., Orr, J.F., Farrar, D.F., Dickson, G.R., 2004b. Degradation of poly-L-lactide.

Part 2: Increased temperature accelerated degradation. Proc. Inst. Mech. Eng. Part H J. Eng. Med. 218, 321–330. https://doi.org/10.1243/0954411041932809

Wise, J., Gillen, K.T., Clough, R.L., 1995. An ultrasensitive technique for testing the Arrhenius extrapolation assumption for thermally aged elastomers. Polym. Degrad. Stab. 49, 403–418. https://doi.org/10.1016/0141-3910(95)00137-B

Zilberman, M., Nelson, K.D., Eberhart, R.C., 2005. Mechanical properties andin vitro degradation of bioresorbable fibers and expandable fiber-based stents. J. Biomed. Mater. Res. Part B Appl. Biomater. 74B, 792–799. https://doi.org/10.1002/jbm.b.30319